Organic & Biomolecular Chemistry

PAPER

View Article Online
View Journal | View Issue

Cite this: *Org. Biomol. Chem.*, 2014, **12**, 3406

Dual-color imaging of cytosolic and mitochondrial zinc ions in live tissues with two-photon fluorescent probes†

Kailash Rathore,‡ Chang Su Lim,‡ Young Lee and Bong Rae Cho*

Received 14th January 2014,
Accepted 24th March 2014

DOI: 10.1039/c4ob00101j

www.rsc.org/obc

We report two-photon probes for Zn^{2+} ions that can simultaneously detect cytosolic and mitochondrial Zn^{2+} ions in live cells and living tissues at 115 mm depth by dual-color TPM imaging with minimum interference from other biologically relevant species.

Introduction

The zinc ion is an essential trace metal ion that plays important roles in mammalian cells as catalytic or structural cofactors.[1] The total zinc ion content in mammalian cells is approximately 0.2 mM, of which a small fraction exists as cytosolic free Zn^{2+} ($[Zn^{2+}]_{cyto}$).[2] Since a low nanomolar concentration of free Zn^{2+} can be cytotoxic, Zn^{2+} homeostasis must be tightly controlled for proper cell function.[1] If the $[Zn^{2+}]_{cyto}$ level is elevated, the excess Zn^{2+} is removed by transferring Zn^{2+} to the extracellular space and shuffling Zn^{2+} to subcellular stores such as endoplasmic reticulum (ER) and mitochondria.[3] To visualize such processes in a live tissue, it is crucial to develop efficient two-photon (TP) probes exhibiting significant TP action cross section ($\Phi\delta_{max}$) values that can simultaneously detect the Zn^{2+} in different organelles by two-photon microscopy (TPM). TPM, which utilizes two near-infrared photons as the excitation source, has become an indispensable tool in biomedical research due to the capability of visualizing the targets deep inside a live tissue with intrinsically localized emission for a long period of time.[4]

Recently, TP probes for Zn^{2+} ions that can independently detect Zn^{2+} in the cytoplasm and mitochondria were reported.[5,6] However, simultaneous detection of Zn^{2+} in the two organelles was not possible, due to the lack of probes for such a purpose. Moreover, it is a crucial task to develop organelle-specific probes that emit fluorescence over a wide range of wavelengths for multi-color imaging. We, therefore, have developed TP probes for cytosolic (BZn-Cyto) and mitochondrial Zn^{2+} ($[Zn^{2+}]_{mito}$) (FZn-Mito), which emit TPEF at widely-separated wavelength regions upon binding with Zn^{2+} (Chart 1). BZn-Cyto was derived from 6-(benzo[*d*]oxazol-2′-yl)-2-(*N*,*N*-dimethylamino)naphthalene (BODAN) as the fluorophore and 2-methoxy-*N*-{2-[*N*,*N*′-bis(2-picolyl)]aminoethyl}-1,4-phenylenediamine (BPEA) as a Zn^{2+} chelator, while FZn-Mito was derived from 7-(benzo[*d*]thiazol-2-yl)-9,9-dimethyl-9*H*-fluorene (BMF) as the reporter, 2-methoxy-*N*-{2-[*N*′-(2-picolyl)-*N*′-(2-pyridin-2-yl)ethyl]aminoethyl}-1,4-phenylenediamine (PPEA) as a Zn^{2+} chelator, and the triphenylphosphonium ion as the mitochondrial targeting moiety.[7] We have employed BODAN and BMF as TP fluorophores because they exhibited significant $\Phi\delta_{max}$ values and emitted TPEF at 470 and 550 nm in aqueous buffer,[8,9] respectively, and we have adopted BPEA and PPEA as the Zn^{2+} receptors from our earlier work because their K_d values are 0.5 and 21 nM, respectively,[5] which are within the range of expected Zn^{2+} concentrations in the two organelles.[6]

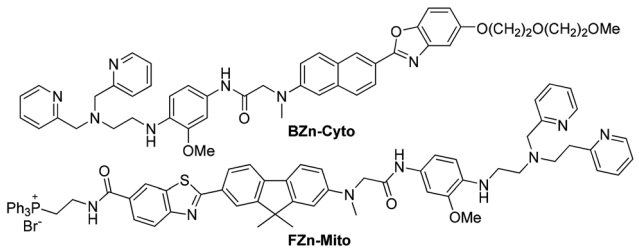

Chart 1 Structures of BZn-Cyto and FZn-Mito.

Results and discussion

Synthesis

Synthesis of BZn-Cyto is summarized in Scheme 1.

Compound **2** was prepared by the Pd-catalyzed coupling of **1** with 5-methoxybenzo[*d*]oxazole. Compound **3** was obtained by the reaction of **2** with BBr_3. BZn-Cyto was prepared by HATU

Department of Chemistry, Korea University, 1-Anamdong, Seoul, Korea.
E-mail: chobr@korea.ac.kr; Fax: (+82) 2-3290-3544; Tel: (+82) 2-3290-3129

† Electronic supplementary information (ESI) available: Experimental details for the synthesis, photophysical studies, and cell imaging. See DOI: 10.1039/c4ob00101j

‡ K.R. and C.S.L. contributed equally.

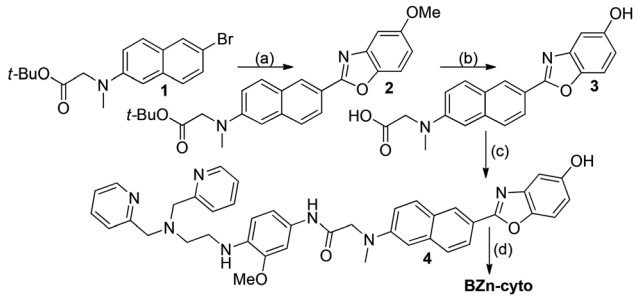

Scheme 1 (a) 5-Methoxybenzo[*d*]oxazole, $Pd(OAc)_2$, *t*-Bu_3P, CuBr, Cs_2CO_3, toluene, 90 °C, 16 h, 56%; (b) BBr_3, CH_2Cl_2, −78 °C–rt, 16 h, 63%; (c) HATU, DIPEA, BPEA, DMF, rt, 16 h, 37%; (d) $CH_3OCH_2CH_2$-OCH_2CH_2OTs, K_2CO_3, DMF, rt, 22 h, 61%.

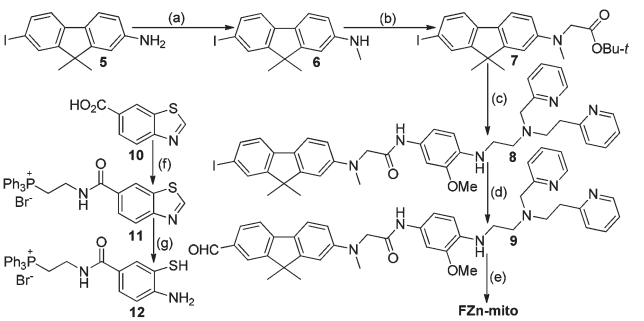

Scheme 2 (a) CH_3I, K_2CO_3, DMF, 0 °C, 5 h, 41%; (b) $BrCH_2CO_2$-*t*-Bu, proton sponge, CH_3CN, reflux, 6 h, 87%; (c) (i) TFA–CH_2Cl_2 (1/1), 0 °C–rt, 5 h; (ii) HATU, DIPEA, PPEA, DMF, rt, 16 h, 53% (over two steps); (d) i-PrMgCl·LiCl, DMF, THF, 0 °C–rt, 4.5 h, 43%; (e) **12**, *p*-toluenesulfonic acid, $CHCl_3$, reflux, 16 h, 25%; (f) DCC, HOBT, CH_2Cl_2, rt, 16 h, 63%; (g) hydrazine monohydrate, EtOH, 80 °C, 3 h, 47%.

coupling of **3** with BPEA to obtain **4** followed by alkylation with 2-(2-methoxyethoxy)ethyl tosylate.

FZn-Mito was prepared by the multi-step synthesis as shown in Scheme 2. N-methylation of **5** followed by alkylation of **6** with *t*-butyl bromoacetate produced **7**. The *t*-Bu group was removed and the resulting carboxylic acid derivative was coupled with PPEA to obtain **8**. Compound **8** was then formylated to afford **9**. FZn-Mito was synthesized by the reaction between **9** and **12**, which was prepared by DCC coupling of **10** with (2-aminoethyl)triphenylphosphonium bromide followed by cleavage of the thiazol ring in **11** (see ESI† for details).

Photophysical properties

The solubilities of BZn-Cyto and FZn-Mito in 3-(*N*-morpholino)-propanesulfonic acid (MOPS) buffer (30 mM MOPS, 100 mM KCl, pH 7.2) as determined by the fluorescence method[10] were approximately 10 and 14 nmol, which correspond to 5 and 7 μM in MOPS buffer, respectively (Fig. S1†). In MOPS buffer, BZn-Cyto and FZn-Mito showed absorption maxima (λ_{max}) at 367 ($\varepsilon = 2.35 \times 10^4$ M^{-1} cm^{-1}) and 392 nm ($\varepsilon = 1.32 \times 10^4$ M^{-1} cm^{-1}), and emission maxima (λ^{fl}_{max}) at 470 (Φ = 0.025) and 559 nm (Φ = 0.023), respectively (Table S1†). The λ_{max} remained nearly the same, while the λ^{fl}_{max} of BZn-Cyto and

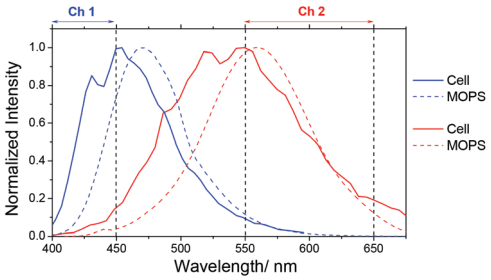

Fig. 1 (a) Normalized one-photon (dotted line) and two-photon excited fluorescence spectra (solid line) of BZn-Cyto (blue) and FZn-Mito (red) measured in MOPS buffer and HeLa cells, respectively. The excitation wavelengths for the one-photon and two-photon processes were 380 and 750 nm, respectively.

FZn-Mito increased gradually by 49 and 73 nm, respectively, as the solvent polarity was increased in the order, 1,4-dioxane < dioxane–EtOH (1/1) < DMF < MOPS containing 1.5 mM sodium dodecylsulfate (MOPS/SDS) < EtOH < MOPS (Fig. S2 and Table S1†).

Upon 750 nm TP excitation in a scanning lambda mode, HeLa cells labeled with BZn-Cyto and FZn-Mito emitted broad spectra with emission maxima at 450 and 530 nm, respectively, which are slightly blue-shifted from those measured in MOPS buffer (Fig. 1). This outcome indicates that the microenvironments of the probes in the organelles are more hydrophobic than MOPS buffer. Moreover, the TPEF spectrum of BZn-Cyto was similar to those measured in EtOH (λ^{fl}_{max} = 445 nm) and DMF (λ^{fl}_{max} = 451 nm), whereas that of FZn-Mito was similar to those measured in MOPS/SDS (λ^{fl}_{max} = 520 nm) and dioxane–EtOH (1/1) (λ^{fl}_{max} = 536 nm) (Fig. 1, S2 and Table S1†), respectively. This result indicates that EtOH and DMF can reasonably represent the microenvironment of BZn-Cyto, while MOPS/SDS and dioxane–EtOH (1/1) are good models for that of FZn-Mito.

Fluorescence titration

We next conducted the fluorescence titration for the complexation reaction of BZn-Cyto and FZn-Mito with Zn^{2+}. When small increments of free Zn^{2+} were added to BZn-Cyto in MOPS buffer, the TP excited fluorescence (TPEF) intensity increased gradually with the metal ion concentration (Fig. 2a), presumably because of the blocking of the photo-induced electron transfer (PeT) process by metal ion complexation.[11] Nearly identical results were observed in the one-photon (OP) process (Fig. S3a†). The fluorescence enhancement factors [FEF = $(F - F_{min})/F_{min}$] of BZn-Cyto measured by OP and TP processes were 27 and 28 in the presence of 22 nM Zn^{2+}, respectively, indicating a high sensitivity of BZn-Cyto to changes in the Zn^{2+} concentration (Table 1). Moreover, the titration curves fitted well with a 1 : 1 binding model (Fig. 2b), the Hill plot was linear with a slope of 1.0 (Fig. 2c), and the Job plot exhibited a maximum point at the mole fraction 0.50 (Fig. S3b†), indicating 1 : 1 complexation between the probe and Zn^{2+}.[12]

The fluorescence titration of FZn-Mito with Zn^{2+} was conducted in MOPS/SDS, which is a good model for the intracellu-

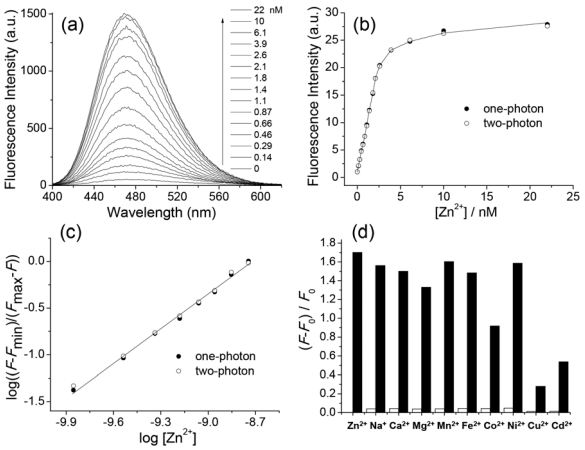

Fig. 2 (a) Two-photon fluorescence spectra of 3 μM BZn-Cyto in the presence of free Zn^{2+} (0–22 nM). (b) One-photon (●) and two-photon (○) fluorescence titration curves for the complexation of BZn-Cyto with free Zn^{2+} (0–22 nM). (c) Hill plots for the complexation of BZn-Cyto with free Zn^{2+} (0–22 nM) measured by one-photon and two-photon processes. (d) The relative fluorescence intensity of 3.0 μM of BZn-Cyto in the presence of 5.0 mM for Na^+, K^+, Ca^{2+}, Mg^{2+}; 300 μM for Mn^{2+}, Fe^{2+}, Co^{2+}, Ni^{2+}, Cu^{2+}, Cd^{2+} (empty bars) followed by addition of 22 nM of free Zn^{2+} (filled bars). All data were collected in MOPS buffer. The excitation wavelengths for one-photon and two-photon processes were 367 and 750 nm, respectively.

Table 1 Photophysical properties of BZn-Cyto and FZn-Mito[a]

Compd.	$\lambda_{max}/\lambda_{fl}$ [b]	Φ [c]	$\lambda^{(2)}_{max}$ [d]	$\Phi\delta_{max}$ [e]	FEF^{TP} [f]	K_d^{TP} [g]
BZn-Cyto	367/470	0.025	740	103[h]	27	1.8
FZn-Mito	392/559	0.023	800[i]	80[i]	16	17

[a] All measurements were made in MOPS buffer (BZn-Cyto) and MOPS/SDS (FZn-Mito) unless otherwise noted. [b] λ_{max} of the one-photon absorption and emission spectra in nm. [c] Fluorescence quantum yield. The uncertainty is ±15%. [d] λ_{max} of the two-photon excitation spectra in nm. [e] Two-photon action cross section measured in the presence of excess Zn^{2+} in 10^{-50} cm^4 s per photon (GM), ±15%. [f] Fluorescence enhancement factors measured by the two-photon process. [g] Dissociation constants for Zn^{2+} measured by the two-photon process in nM, ±10%. [h] The $\Phi\delta_{max}$ value was 135 GM in EtOH. [i] The solvent was dioxane–EtOH (1/1).

lar environment (see above). The titration behavior was similar to that for BZn-Cyto; that is, the OP and TP titration curves fitted well with the 1 : 1 binding model with FEF^{TP} = 16 and FEF^{OP} = 16 in the presence of 130 nM Zn^{2+} (Fig. S4a–c†). The Hill plots (Fig. S4d†) and the Job plots (Fig. S4e†) also indicated 1 : 1 complexation between the probe and Zn^{2+}.[12] The dissociation constants (K_d^{TP}) for the complexation reactions of BZn-Cyto and FZn-Mito with Zn^{2+} in a TP mode were calculated by the literature method (Fig. 1b and S4c†).[13,14] The K_d^{TP} values of BZn-Cyto and FZn-Mito were 1.8 ± 0.3 and 17 ± 2 nM, respectively (Table 1).

Selectivity

We then studied the selectivity of BZn-Cyto and FZn-Mito for Zn^{2+}. BZn-Cyto showed a high selectivity for Zn^{2+}, as revealed by the negligible fluorescence intensity in the presence of 5 mM concentration of Na^+, Ca^{2+}, and Mg^{2+} and 300 μM of Mn^{2+}, Fe^{2+}, Co^{2+}, Ni^{2+}, Cu^{2+}, and Cd^{2+}, as well as a large enhancement in the fluorescence intensity upon the addition of 22 nM of Zn^{2+} (Fig. 1d). Although the selectivity of BZn-Cyto for Zn^{2+} over Co^{2+}, Cu^{2+}, and Cd^{2+} is not as high as that over other metal ions, it will not be a problem because the intracellular concentration of these metal ions should be much lower than 300 μM. A similar result was observed for FZn-Mito (Fig. S4f†). In addition, BZn-Cyto and FZn-Mito were relatively pH-insensitive at pH > 4.0 (Fig. S5†). These results established that BZn-Cyto and FZn-Mito can detect Zn^{2+} with minimum interference from other competing metal ions and pH.

Two-photon action cross section

We next evaluated the abilities of BZn-Cyto and FZn-Mito to detect Zn^{2+} in a TP mode. The TP action cross sections ($\Phi\delta_{max}$) of BZn-Cyto and FZn-Mito were measured by the fluorescence method.[15,16] The $\Phi\delta_{max}$ values of BZn-Cyto were 4 GM in the absence and 103 GM at 740 nm in the presence of excess Zn^{2+} in MOPS buffer (Fig. 3 and Table 1). The value increased to 135 GM in EtOH in the presence of excess Zn^{2+} (Fig. 3 and Table 1), presumably because of the enhanced fluorescence quantum of the BZn-Cyto yield (0.68 in MOPS *vs.* 0.90 in EtOH) in a less polar solvent (Table S1†). Since it was difficult to measure the $\Phi\delta_{max}$ value of FZn-Mito in MOPS/SDS due to the scattering of TPEF signals by the SDS aggregates, the $\Phi\delta_{max}$ value was determined in dioxane–EtOH (1/1), which is a good model for the intracellular environment (see above). The $\Phi\delta_{max}$ value of FZn-Mito in dioxane–EtOH (1/1) was 80 GM in the presence of excess Zn^{2+}. These values allowed us to obtain bright TPM images of the probe-labeled cells and tissues by TPM using BZn-Cyto and FZn-Mito as the TP probes.

Detection of Zn^{2+} ions in a live cell

We then sought to apply BZn-Cyto and FZn-Mito as TP probes for detecting $[Zn^{2+}]_{cyto}$ and $[Zn^{2+}]_{mito}$ in cellular environments by dual-color imaging. The TPM images of the HeLa cells

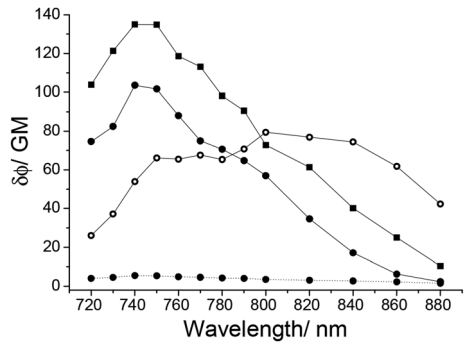

Fig. 3 Two-photon action spectra of BZn-Cyto in EtOH (■) and MOPS buffer (●) and of FZn-Mito in 1,4-dioxane–EtOH (1/1) (○) in the absence (dotted line) and presence (solid line) of excess Zn^{2+}.

labeled with BZn-Cyto and FZn-Mito were bright, presumably because of the easy loading and large $\Phi\delta_{max}$ values. Since the TPEF spectra of BZn-Cyto and FZn-Mito measured in HeLa cells showed appreciable overlap, we chose half of the bands, that is, 400–450 nm (Ch1, BZn-Cyto) and 550–650 nm (Ch2, FZn-Mito), as the detection windows (Fig. 1). Under these conditions, the TPEF of FZn-Mito contributed 6% of the total TPEF in Ch1, while that of BZn-Cyto contributed 4% of the total TPEF in Ch2. Hence, it was possible to simultaneously detect $[Zn^{2+}]_{cyto}$ and $[Zn^{2+}]_{mito}$ by dual-color imaging with minimum interference from each other.

To test whether FZn-Mito can specifically stain the mitochondria, we performed a co-localization experiment with the HeLa cells co-labeled with FZn-Mito and MitoTracker Red FM (MTR), a commercially available one-photon probe for mitochondria, by using the detection windows at 550–650 (FZn-Mito) and 600–700 nm (MTR), respectively (Fig. S6†). Since FZn-Mito did not emit fluorescence and the TPEF of MTR was not detected at 450–550 nm when excited at 543 and 800 nm, respectively, the co-localization experiment could be conducted without interference from each other (Fig. 4d).[17] The TPM image matched well with the OPM image of mitochondria. The Pearson's colocalization coefficient (A), which describes the correlation of the intensity distribution between the channels,[18] of FZn-Mito with MitoTracker Red FM was 0.86, indicating that FZn-Mito exists predominantly in mitochondria (Fig. 4).

To confirm whether the bright regions reflected $[Zn^{2+}]_{cyto}$ and $[Zn^{2+}]_{mito}$, we treated the HeLa cells co-labeled with BZn-Cyto and FZn-Mito with 2,2′-dithiodipyridine (DTDP; 150 μM), a reagent that promotes the release of Zn^{2+} from Zn^{2+}-binding proteins,[19] and carbonyl cyanide *m*-chlorophenylhydrazone (CCCP; 10 μM), a reagent that collapses mitochondrial potential and then depolarizes the plasma membrane, thereby releasing the Zn^{2+} into the extracellular space (Fig. 5).[20] In both channels, the TPEF intensities increased upon addition of DTDP and decreased upon treatment with CCCP. The only difference was the higher sensitivity of BZn-Cyto to the stimuli that can be attributed to its smaller K_d^{TP} value. It was not possible to visualize the transport of Zn^{2+} between the two regions probably because the process was too fast to monitor with our instrument. Nevertheless, BZn-Cyto and FZn-Mito were clearly capable of detecting $[Zn^{2+}]_{cyto}$ and $[Zn^{2+}]_{mito}$ in live cells by dual-color TPM imaging (Fig. 5h). Moreover, the assays with a CCK-8 kit revealed that both probes exhibited low cytotoxicity (Fig. S7†). Further, the TPEF intensity at a given spot on the HeLa cells labeled with BZn-Cyto and FZn-Mito remained nearly the same after continuous irradiation of the fs-pulses for 1 h, indicating their high photostabilities (Fig. S8†). These results established that BZn-Cyto and FZn-Mito can simultaneously detect $[Zn^{2+}]_{cyto}$ and $[Zn^{2+}]_{mito}$ by dual-color TPM imaging for a long period of time with

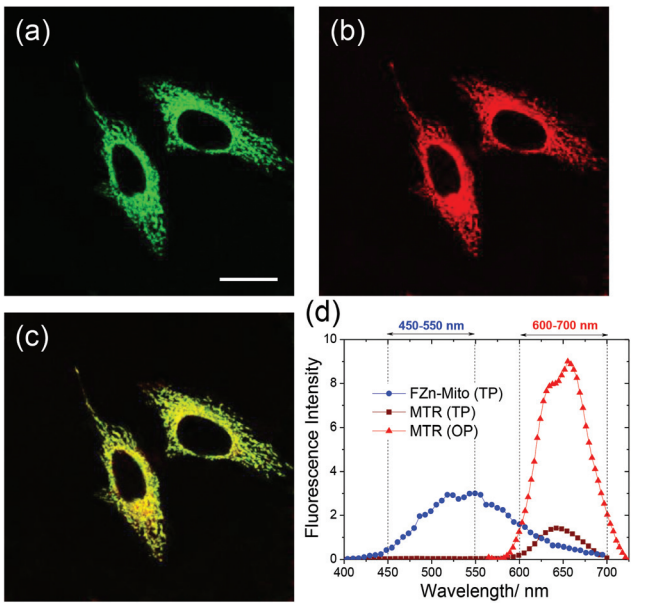

Fig. 4 (a) TPM and (b) OPM images of HeLa cells co-labeled with FZn-Mito (3 μM) and MTR (1 μM). (c) Colocalized image. (d) Two-photon and one-photon excited fluorescence spectra of FZn-Mito and MTR collected from (a) and (b). FZn-Mito did not emit fluorescence when excited at 543 nm. The wavelengths for one-photon and two-photon excitation were 543 and 800 nm, respectively, and the emission was collected at 450–550 nm (a) and 600–700 nm (b), respectively. Scale bar: 25 μm.

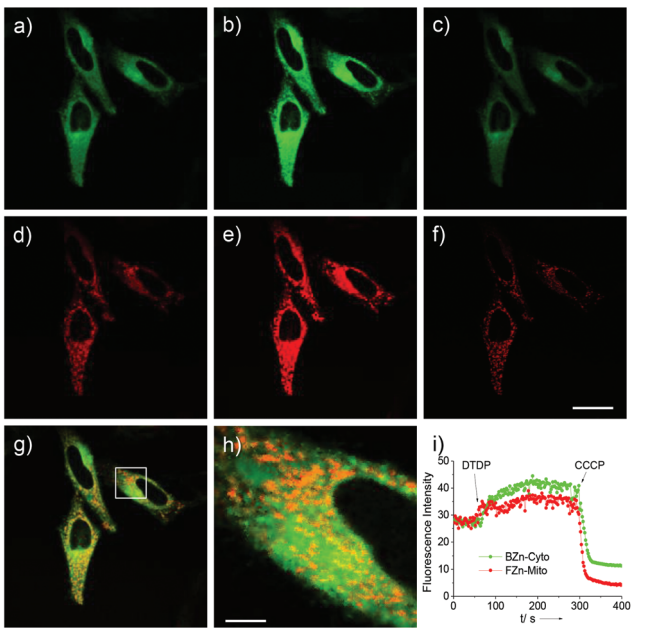

Fig. 5 TPM images of HeLa cells co-labeled with BZn-Cyto (3 μM) and FZn-Mito (3 μM) collected at Ch1 (a–c) and Ch2 (d–f), respectively. Images were obtained before (a, d) and after (b, e) addition of 150 μM DTDP. (c, f) After addition of 10 μM CCCP to (b, e). (g) Merged image of (a) and (d). (h) Enlarged images of the white box in (g). (i) Relative TPEF intensity of HeLa cells co-labeled with BZn-Cyto and FZn-Mito as a function of time. The excitation wavelength was 750 nm and TPEF intensities were collected at Ch1 (BZn-Cyto) and Ch2 (FZn-Mito), respectively. Scale bars: (f) 30 and (h) 5 μm.

minimum interference from other competing metal ions, pH, and cytotoxicity.

Detection of Zn^{2+} ions in a live tissue

We next assessed the ability of BZn-Cyto and FZn-Mito to detect Zn^{2+} deep inside live tissue. For this experiment, the hippocampus was isolated from a 2-week-old rat, and a slice was incubated with 20 μM of BZn-Cyto and FZn-Mito for 1 h at 37 °C. Since it took a longer time to stain the tissues than cells during which time they may be deformed, excess amounts of BZn-Cyto and FZn-Mito were used to facilitate staining. The bright-field image of a part of this slice revealed the CA2 and CA3 regions (Fig. 6g). The TPM images collected at Ch1 and Ch2 revealed the distribution of $[Zn^{2+}]_{cyto}$ and $[Zn^{2+}]_{mito}$ in the same region (Fig. 6a,b and d,e). At a higher magnification $[Zn^{2+}]_{cyto}$ and $[Zn^{2+}]_{mito}$ distribution could be clearly visualized at 115 mm depth in a live tissue (Fig. 6f). Moreover, the TPEF intensity increased upon addition of 300 μM DTDP, and it decreased upon treatment with 10 μM CCCP (Fig. 6h), a result similar to that observed in the cells. These findings confirmed that BZn-Cyto and FZn-Mito can simultaneously detect the $[Zn^{2+}]_{cyto}$ and $[Zn^{2+}]_{mito}$ in live tissues at 115 mm depth by dual-color TPM imaging.

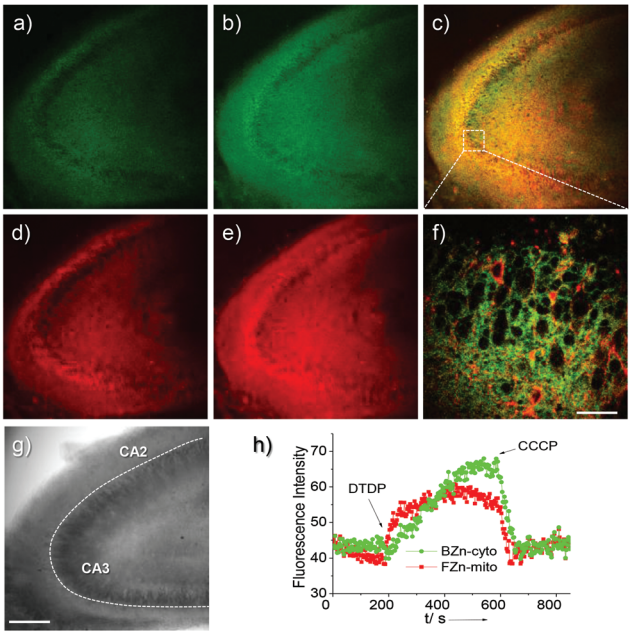

Fig. 6 (a–f) TPM image of a rat hippocampal slice co-stained with 20 μM each of BZn-Cyto and FZn-Mito collected at Ch1 (a, b) and Ch2 (d, e), respectively. (c) Merged image of (b) and (e). TPM images were acquired before (a, d) and after (b, e) addition of DTDP by 10× magnification. (f) Magnification at 100× in the pyramidal neuron layer of CA3 regions (white box in (c)) at a depth of 115 μm. (g) Bright-field image of CA2–CA3. (h) Relative TPEF intensity of a rat hippocampal slice co-labeled with BZn-Cyto- and FZn-Mito upon addition of 300 μM DTDP and 10 μM CCCP as a function of time. The excitation wavelength was 750 nm and TPEF intensities were collected at Ch1 (BZn-Cyto) and Ch2 (FZn-Mito), respectively. Scale bars: 30 μm (f, 100×) and 300 μm (g, 10×).

Conclusions

We have developed TP probes for $[Zn^{2+}]_{cyto}$ and $[Zn^{2+}]_{mito}$, which emit TPEF at widely-separated wavelength regions upon binding with Zn^{2+}, and show significant TP cross sections, low cytotoxicity, high photostability, and insensitivity to pH in the biologically relevant pH range. The new probes can simultaneously detect $[Zn^{2+}]_{cyto}$ and $[Zn^{2+}]_{mito}$ in live cells, as well as in living tissues at 115 mm depth by dual-color TPM imaging with minimum interference from other biologically relevant species.

Experimental section

Synthesis

BZn-Cyto. A solution of diethyleneglycol monomethyl ether tosylate (14 mg, 0.050 mmol) in DMF (1 mL) was added dropwise to a mixture of compound **4** (29 mg, 0.042 mmol) and K_2CO_3 (7.0 mg, 0.050 mmol) in DMF (2 mL) at rt under an argon atmosphere. The resulting mixture was stirred for 22 h while TLC examination revealed complete consumption of the starting material. The reaction mixture was diluted with water (10 mL) and extracted with EtOAc (4 × 5 mL). Combined organic extracts were washed with brine (5 mL), dried over anhydrous $MgSO_4$ and filtered. Evaporation of the solvent *in vacuo* afforded a crude residue which was purified by silica gel column chromatography using MeOH–$CHCl_3$–acetone (1/9/10) as the eluent to furnish BZn-Cyto (20 mg, 0.025 mmol) in 61% yield as a colorless viscous oil. ^{1}H NMR (300 MHz, $CDCl_3$): 8.61 (s, 1H), 8.52–8.48 (m, 2H), 8.20 (dd, J = 8.8, 2.2 Hz, 1H), 8.11 (s, 1H), 7.89 (d, J = 8.8 Hz, 1H), 7.79 (d, J = 8.8 Hz, 1H), 7.66–7.58 (m, 2H), 7.52–7.43 (m, 4H), 7.18 (dd, J = 8.8, 2.2 Hz, 1H), 7.16–7.07 (m, 3H), 6.97 (dd, J = 8.8, 2.2 Hz, 1H), 6.70 (dd, J = 8.8, 2.2 Hz, 1H), 6.38 (d, J = 8.8 Hz, 1H), 4.21 (t, J = 6.0 Hz, 2H), 4.10 (s, 2H), 3.94–3.81 (m, 9H), 3.78–3.72 (m, 2H), 3.63–3.57 (m, 2H), 3.40 (s, 3H), 3.23 (s, 3H), 3.16 (t, J = 6.0 Hz, 2H), 2.86 (t, J = 6.0 Hz, 2H). ^{13}C NMR (100 MHz, acetone-d_6): 169.1, 166.1, 161.5, 158.7, 151.2, 150.7, 148.5, 147.2, 145.2, 138.5, 138.0, 137.2, 131.8, 130.3, 129.3, 128.8, 128.1, 126.0, 124.7, 123.8, 122.3, 118.6, 115.4, 114.3, 112.3, 110.9, 108.0, 105.5, 105.2, 73.7, 72.2, 71.3, 70.2, 61.8, 59.8, 58.9, 56.9, 54.5, 42.8, 41.2. HRMS (FAB): calcd for $C_{46}H_{50}N_7O_6$ $[M + H]^+$: 796.3823, Found 796.3820.

FZn-Mito. A solution of amino thiol **12** (19 mg, 0.035 mmol) in $CHCl_3$ (1 mL) was added dropwise to a stirred solution of aldehyde **9** (24 mg, 0.035 mmol) and *p*-toluenesulfonic acid monohydrate (PTSA, 2 mg, 0.0003 mmol) in $CHCl_3$ (4 mL) under an argon atmosphere. The reaction mixture was refluxed for 16 h while accumulation of a brown solid was observed on the wall of the RB flask. Mother liquor containing the desired product was decanted carefully and the solid residue was rinsed twice with cold $CHCl_3$ (2 × 3 mL). Evaporation of the solvent under reduced pressure yielded a crude residue which was purified by reverse-phase HPLC using the following conditions: YMC-Pack ODS-A, (20 × 250 mm), 5 μm, 12 nm;

mobile phase, MeOH–H_2O (0.1% TFA) = 20/80 to 100/0 to 100/0 (linear gradient, 60 then 70 min); flow rate, 8 mL min^{-1}; temperature, 40 °C; injection, 0.1 mL, detection, UV (210 nm). The fraction of interest at retention time 49.5 min was collected and lyophilized to furnish FZn-mito (9 mg, 0.007 mmol) in 21% yield as a dark brown, gummy product. ^{1}H NMR (400 MHz, acetone-d_6): δ 8.61–8.49 (m, 2H), 8.23 (s, 1H), 8.14–7.99 (m, 10H), 7.99–7.90 (m, 4H), 7.90–7.68 (m, 11H), 7.54 (d, J = 7.8 Hz, 1H), 7.45–7.34 (m, 2H), 7.11–6.99 (m, 2H), 6.82 (d, J = 7.8, 1H), 6.65 (d, J = 7.8, 1H), 4.65 (s, 2H), 4.18 (s, 2H), 4.09–3.85 (m, 6H), 3.84–3.65 (m, 7H), 3.65–3.51 (m, 2H), 3.23 (s, 3H), 1.56 (s, 6H). ^{31}P NMR (162 MHz, DMSO-d_6): 22.3 ppm. HRMS (FAB$^+$): m/z calcd for $[C_{68}H_{66}N_8O_3PS]^+$: 1105.4716, Found 1105.4711.

Spectroscopic measurements

Absorption spectra were recorded on a S-3100 UV-Vis spectrophotometer and fluorescence spectra were obtained with a FluoroMate FS-2 fluorescence spectrometer with a 1 cm standard quartz cell. The fluorescence quantum yield was determined by using coumarin 307 (Φ = 0.95 in MeOH) as the reference by the literature method.[21]

Water solubility

A small amount of dye was dissolved in DMSO to prepare the stock solutions (1.0×10^{-2} M). The solution was diluted to 6.0×10^{-3}–6.0×10^{-5} M and added to a cuvette containing 2.0 mL of buffer (30 mM MOPS, 100 mM KCl, pH 7.2) using a micro syringe. In all cases, the concentration of DMSO in buffer was maintained at 0.2%.[10] The plots of fluorescence intensity against the total amount of the dye injected into the cuvette were linear at low dye content and showed downward curvature as more dye was added (Fig. S1†). The maximum point in the linear region was taken as the solubility. The solubility of BZn-Cyto was 5.0 μM and that of FZn-Mito was 7.0 μM.

Determination of apparent dissociation constants (K_d)

A series of solutions containing various concentrations of free Zn^{2+} ($[Zn^{2+}]_{free}$) was prepared by dissolving various amounts of $ZnSO_4$ (0–9.5 mM) and 10 mM EGTA in MOPS (30 mM, pH 7.2, 0.1 M KCl) by the literature method.[13,22] To determine the K_d values for the probe-Zn^{2+} complexes, the fluorescence titration curves (Fig. 1a and S3b†) were obtained and fitted to the following equation (Fig. 1b):[23,24]

$$F = F_0 + (F_{max} - F_0)\frac{[Zn^{2+}]_{free}}{K_d + [Zn^{2+}]_{free}}$$

where F is the fluorescence intensity, F_{max} is the maximum fluorescence intensity, F_0 is the fluorescence intensity in the absence of Zn^{2+}, and $[Zn^{2+}]_{free}$ is the free Zn^{2+} concentration. The K_d value that best fits the titration curve with the above equation was calculated using the Excel program.

Measurement of two-photon cross section

The two-photon cross sections (δ) were determined by using the femtosecond (fs) fluorescence measurement technique as described.[15] BZn-Cyto and FZn-Mito were dissolved in solvent at concentrations of 3.0×10^{-6} M and then the two-photon induced fluorescence intensity was measured at 720–900 nm by using Rhodamine 6G in MeOH as the reference, whose two-photon property has been well characterized in the literature.[16] The TPA cross section was calculated using $\delta = \delta_r(S_s\Phi_r\phi_r c_r)/(S_r\Phi_s\phi_s c_s)$ where the subscripts s and r stand for the sample and reference molecules, respectively. The intensity of the signal collected using a CCD detector was denoted as S. Φ is the fluorescence quantum yield. ϕ is the overall fluorescence collection efficiency of the experimental apparatus. The number density of the molecules in solution was denoted as c. δ_r is the TPA cross section of the reference molecule.

Cell culture

HeLa human cervical carcinoma cells were obtained from American Type Culture Collection (ATCC, Manassas, VA, USA). The cells were cultured in DMEM (WelGene Inc., Seoul, Korea) supplemented with heat-inactivated 10% FBS (WelGene), penicillin (100 units mL^{-1}), and streptomycin (100 μg mL^{-1}). All the cell lines were maintained in a humidified atmosphere of 5% CO_2 and 95% air at 37 °C. Two days before imaging, the cells were detached and were replaced on glass-bottomed dishes (MatTek). For labeling, the growth medium was removed and replaced with DMEM without FBS. The cells were incubated with BZn-Cyto and FZn-Mito (3 μM) for 30 min at 37 °C. Following this incubation, the cells were washed three times with DMEM without FBS and imaged.

Two-photon fluorescence microscopy

Two-photon fluorescence microscopy images of probe-labeled HeLa cells and tissues were obtained with spectral confocal and multiphoton microscopes (Leica TCS SP2) with a ×10 and ×100 objective, numerical aperture (NA) = 0.30 and 1.30. The two-photon fluorescence microscopy images were obtained with a DM IRE2 Microscope (Leica) by exciting the probes with a mode-locked titanium–sapphire laser source (Coherent Chameleon, 90 MHz, 200 fs) set at wavelength 740 nm and output power 1305 mW, which corresponded to 2.28×10^8 mW nm^{-2} (×10) and 3.80×10^9 mW nm^{-2} (×100) power at the focal plane. To obtain images in the 400–450 nm (channel 1) and 550–650 nm (channel 2) ranges, internal PMTs were used to collect the signals in an 8 bit unsigned 512 × 512 pixels at 400 Hz scan speed.

Co-localization experiments

Co-localization experiments were conducted by co-staining HeLa cells with FZn-Mito (3 μM) and MTR (1 μM) for 30 min. The emission was collected at 550–650 (FZn-Mito) and 600–700 nm (MTR) regions upon excitation at 543 (MTR) and 740 (BZn-Cyto) nm, respectively. The background images were corrected, and the distribution of pixels in the TPM and OPM

images acquired in the shorter and longer wavelength channels, respectively, was compared by using scatter gram. The Pearson's co-localization coefficients were calculated by using the Autoquant X2 program.

Cell viability

The viability of HeLa cells was determined using a CCK-8 kit (Cell Counting Kit-8, Dojindo, Japan) according to the manufacturer's protocol.

Photostability

The photostabilities of BZn-Cyto and FZn-Mito were determined by monitoring the changes in TPEF intensity with HeLa cells chosen without bias.

Preparation and staining of fresh rat hippocampal and hypothalamic slices

Slices were prepared from the hippocampus of a 2-week-old rat (SD). Coronal slices were cut into 400 μm-thick using a vibrating-blade microtome in artificial cerebrospinal fluid (ACSF; 138.6 mM NaCl, 3.5 mM KCl, 21 mM $NaHCO_3$, 0.6 mM NaH_2PO_4, 9.9 mM D-glucose, 1 mM $CaCl_2$, and 3 mM $MgCl_2$). Slices were incubated with 20 μM BZn-Cyto and FZn-Mito in ACSF bubbled with 95% O_2 and 5% CO_2 for 30 min at 37 °C. Slices were then washed three times with ACSF and transferred to glass-bottomed dishes (MatTek) and observed using a spectral confocal two-photon microscope.

Acknowledgements

This work was supported by Korea University, the National Research Foundation (NRF) grant (NRF2012007850), the Basic Science Research Program of the NRF funded by the Ministry of Education (NRF20100020209), and the Korea Healthcare Technology R&D Project, Ministry of Health & Welfare, Republic of Korea (A111182).

Notes and references

1 (*a*) J. L. Vinkenborg, T. J. Nicolson, E. A. Bellomo, M. S. Koay, G. A. Rutter and M. Merkx, *Nat. Methods*, 2009, **6**, 737; (*b*) W. Maret, *Biometals*, 2009, **22**, 149.
2 C. E. Outten and T. V. O'Halloran, *Science*, 2001, **292**, 2488.
3 R. A. Colvin, W. R. Holmes, C. P. Fontaine and W. Maret, *Metallomics*, 2010, **2**, 306.
4 F. Helmchen and W. Denk, *Nat. Methods*, 2005, **2**, 932.
5 A. Antony, C. S. Lim, Y. S. Tian, J. H. Han, M. Y. Kang and B. R. Cho, *Chem. – Asian J.*, 2011, **6**, 1234.
6 G. Masanta, C. S. Lim, H. J. Kim, J. H. Han, H. M. Kim and B. R. Cho, *J. Am. Chem. Soc.*, 2011, **133**, 5698.
7 (*a*) B. C. Dickinson, D. Srikun and C. J. Chang, *Curr. Opin. Chem. Biol.*, 2010, **14**, 50; (*b*) B. C. Dickinson and C. J. Chang, *J. Am. Chem. Soc.*, 2008, **130**, 9638.
8 J. H. Han, S. K. Park, C. S. Lim, M. K. Park, H. M. Kim and B. R. Cho, *Chem. – Eur. J.*, 2012, **18**, 15246.
9 S. K. Das, C. S. Lim, S. Y. Yang, J. H. Han and B. R. Cho, *Chem. Commun.*, 2012, **48**, 8395.
10 H. M. Kim, H. J. Choo, S. Y. Jung, Y. G. Ko, W. H. Park, S. J. Jeon, C. H. Kim, T. Joo and B. R. Cho, *ChemBioChem*, 2007, **8**, 553.
11 R. A. Bissell, E. Calle, A. P. de Silva, S. A. de Silva, H. Q. N. Gunaratne, J.-L. Habib-Jiwan, S. L. A. Peiris, R. A. D. D. Rupasinghe, T. K. S. D. Samarasinghe, K. R. A. S. Sandanayake and J.-P. Soumillion, *J. Chem. Soc., Perkin Trans 2*, 1992, 1559.
12 K. A. Connors, *Binding Constants*, Wiley, New York, 1987.
13 C. J. Fahrni and T. V. O'Halloran, *J. Am. Chem. Soc.*, 1999, **121**, 11448.
14 T. Hirano, K. Y. Urano and T. Nagano, *J. Am. Chem. Soc.*, 2002, **124**, 6555.
15 S. K. Lee, W. J. Yang, J. J. Choi, C. H. Kim, S.-J. Jeon and B. R. Cho, *Org. Lett.*, 2005, **7**, 323.
16 N. S. Makarov, M. Drobizhev and A. Rebane, *Opt. Express*, 2008, **6**, 4029.
17 *A Guide to Fluorescent Probes and Labeling Technologies*, ed. R. P. Haugland, Molecular Probes, Eugene, OR, 10th edn, 2005.
18 K. Emmerson and K. Roehrig, *Comp. Biochem. Physiol., B: Biochem. Mol. Biol.*, 1992, **103**, 663.
19 E. Aizenman, A. K. Stout, K. A. Hartnett, K. E. Dineley, B. McLaughlin and I. J. Reynolds, *J. Neurochem.*, 2000, **75**, 1878.
20 T. Caporale, D. Ciavardelli, C. Di Ilio, P. Lanuti, D. Drago and S. L. Sensi, *Exp. Neurol.*, 2009, **218**, 228.
21 J. N. Demas and G. A. Crosby, *J. Phys. Chem.*, 1971, **75**, 991.
22 M. Taki, J. L. Wolford and T. V. O'Halloran, *J. Am. Chem. Soc.*, 2004, **126**, 712.
23 A. E. Martell and R. M. Smith, *NIST Critical Stability Constants of Metal Complexes. NIST Standard Reference Database 46, Version 7.0*, 2003.
24 T. Hirano, K. Kikuchi, Y. Urano, T. Higuchi and T. Nagano, *J. Am. Chem. Soc.*, 2000, **122**, 12399.

